To be published in the Proceedings of the "4th Intl. Conference on Trends in Welding Research", Gatlinburg, TN, 5-8 June 1995.

Microstructure Evaluation In Low Alloy Steel Weld Metal From Convective Heat Transfer Calculations In Three Dimensions

K. Mundra*, T. DebRoy*, S.S. Babu* and S.A. David#

* Department of Materials Science and Engineering, The Pennsylvania State University, University Park, PA

Metals and Ceramics Division, Oak Ridge National Laboratory, Oak Ridge, TN

ABSTRACT

Heat transfer and fluid flow during manual metal arc welding of low alloy steels were investigated by solving the equations of conservation of mass, momentum and energy in three dimensions. The cooling rates were calculated at various locations in the weldment. Calculated cooling rates were coupled with an existing phase transformation model to predict the percentages of acicular, allotriomorphic and Widmanstätten ferrites in various low alloy steel welds containing different concentration of vanadium and manganese. The computed microstructures were found to be in good agreement with the experimentally observed microstructures. The agreement indicates significant promise for predicting weld metal microstructure from the fundamentals of transport phenomena.

THE INTEGRITY AND PERFORMANCE of a welded joint depends on microstructure and properties [1,2] of the weldment. During welding, the interaction of the heat source and the material leads to rapid heating, melting and vigorous circulation of the liquid metal in the weld pool. As the heat source moves away from the molten pool, solidification of the material occurs. The resulting thermal cycle plays an important role in determining the weld structure and properties.

An accurate prediction of the thermal cycle in the weldment is a prerequisite for the prediction of microstructural constituents in various regions of the weldment. Direct accurate measurements of temperature profiles in a weld pool are difficult. Furthermore, noncontact techniques for the measurement of temperature profiles in the weld pool are still evolving [3]. Earlier models to calculate temperature-time history in the welds were based on the solution of conservation of energy [4-6] and neglected the effect of fluid flow in the weld pool. Fluid flow in the weld pool may affect the time-temperature history experienced by a weld metal.

In the past decade, significant progress has been made in the solution of equations describing conservation of mass, momentum and energy in the weld pool [7-11]. The role of Marangoni, electromagnetic and the buoyancy forces on the weld pool geometry has been investigated [7,8]. The effect of surface active elements on the transient development of weld pool geometry has also been examined in details [12]. Simple features of solidification structure such as secondary dendrite arm spacing have been predicted from the cooling rate data calculated from fundamentals of transport phenomena [9]. These developments have provided significant insight into the welding process. However, accurate transient temperature calculations from comprehensive fluid flow and heat transfer models have not been used to predict fusion zone microstructures. The work reported here was aimed at predicting volume percentages of acicular, allotriomorphic and Wimanstätten ferrites in various low alloy steel welds using detailed three dimensional transient temperature calculations from a heat transfer and fluid flow model in the weld pool and phase transformation theories of low alloy steels.

MODEL FRAMEWORK

Assumptions in the Model Formulation. During manual metal arc welding, the energy is transferred to the workpiece both from the arc and from the metal droplets generated from the consumable electrode. The energy distribution from the arc does not change significantly with time and the distribution is Gaussian in nature in most cases. However, the energy transfer from the droplets depends on various parameters such as the drop frequency, the drop transfer mode, and their shape, size and temperature. Because of the transient nature of these parameters and the resulting complexity in integrating these phenomena in the numerical scheme, a time average energy transfer rate was considered in the model. Since all the droplets do not impinge exactly on the same location on the weld pool surface, the time average energy density distribution was assumed to be Gaussian in its spatial distribution. The energy distributions from the arc and metal droplets from the electrode, were coupled together and expressed in the form of an overall energy transfer efficiency. In principle, the shape of the energy density distribution profiles for the arc and for the metal drops may be different. Our assessment of this effect,

considering different energy distributions, resulted in somewhat different peak temperatures and minor change in the weld geometry. However, no significant difference in temperature-time history was observed in the range of 1100 to 700 K. The temperature time history in this temperature range governs the microstructural development in low alloy steel weldments [13]. Therefore, the time average values of the energy transport, assumed in the formulation of the model, is justified for the purpose of this research. For simplicity, the weld pool surface was considered to be flat. The fluctuations in the mass of the weld pool due to droplet addition was approximated by a time average constant mass of the metal in the weld pool.

The transport of momentum from the droplets to the weld pool was ignored. The resulting inaccuracy in the cooling rate in the fusion zone in the 1100 to 700 K range depends on the magnitude of the Peclet number for heat transfer and its change due to additional momentum from the metal drops. At low values of Pe (< 0.5), the impact of momentum from the droplets is negligible. However, at high values of Pe (=60), a 17% change in Pe resulting from the momentum transfer from the droplets leads to roughly 1.5% change in the average cooling rate in the 1100 to 700 K range.

The spatial variation of the inclusion characteristics and the effects of this variation on the microstructure development are ignored. It should be noted that the detailed theoretical models to describe the development of inclusions are still evolving [14,15]. Furthermore, the elemental segregation [16] was not considered in the microstructure model. The preceding discussion indicates both the complexity of welding process and the need for the simplification to keep the computational task within practical limits.

Fluid Flow and Heat Transfer in the Weld Pool. The welding process is transient when viewed in a stationary coordinate system (x,y,z). This transient problem can be transformed to a steady state problem by solving in a coordinate system that moves with the heat source (ξ,y,z), where $\xi = x + U_s t$ and U_s is the scanning velocity. A new numerical methodology that accounts for the transport of mass, momentum and energy due to the moving heat source by suitably defining terms in the governing equations has been developed. The methodology involves the transformation $V' = V + U_s$ where V' is the velocity at any point with respect to the frame attached to the heat source and V is the convective component of the velocity. The details of this methodology will be published elsewhere [17,18]. However, the final equations of mass, momentum, and energy conservation in the ξ,y,z coordinate are given here:

Equation of Continuity

$$\nabla . V = 0 \qquad (1)$$

where V (U, V, W) is the velocity vector. The density, ρ, is assumed to be constant.

Momentum Equations

$$\rho\nabla(V.V) = -\nabla P + \mu\nabla.(\nabla V) + \left(S_v - \rho\nabla.(UV)\right) \qquad (2)$$

where U_s is the scanning velocity, μ is the viscosity, P is the effective pressure and S_V is the source term that takes into account the combined effect of buoyancy force, F_b, Marangoni stress, τ, and electromagnetic force, F_e.

Energy Equation

The technique used here to account for the phase change has evolved from the work of Voller and Prakash [19]. The total enthalpy of the material, H, is represented as a sum of sensible heat, $h = \int C_p dT$, and latent heat content, ΔH. The energy equation is written as follows:

$$\rho\nabla.(Vh) = \nabla.\left(\frac{k}{C_p}\nabla h\right) + S_l + S_h - \rho\nabla.(Uh) \qquad (3)$$

where C_P is specific heat, k is thermal conductivity, S_h is the source term that takes into account the heat input from the welding source and the convective and radiative heat loss and S_l is the source term that accounts for latent heat of melting and convective transport of latent heat and is given by [19] :

$$S_l = \rho\nabla.(V\Delta H) + \rho\nabla.(U\Delta H) \qquad (4)$$

where $\Delta H = F(T)$, the latent heat content, is defined as a function of the temperature and is given by:

$$\begin{aligned} F(T) &= L && T > T_l \text{ and} \\ F(T) &= L\left(\frac{T - T_s}{T_l - T_s}\right) && T_s \le T \le T_l, \\ F(T) &= 0 && T < T_l \end{aligned} \qquad (5)$$

where L is the latent heat, T_l is the liquidus temperature and T_s is the solidus temperature.

Boundary Conditions and Source Terms. The calculations were done only for half of the work piece, since there is a symmetry about y=0 plane. Along the plane of symmetry, V and the gradients of U and W were defined as zero. Since the weld pool surface was assumed to be flat, W was defined to be zero at the top surface. The condition that the velocity is zero in the mushy region is accounted by making use of enthalpy-porosity technique [19]. The natural convection effect is taken into account by defining the buoyancy source term, S_b, to be (Boussinesq approximations):

$$S_b = \rho g\beta(T - T_{ref}) \qquad (6)$$

where β is the thermal expansion coefficient of liquid and T_{ref} is the reference temperature.

Since the temperature varies on the surface of the weld pool, a shear stress (Marangoni stress) is produced on the free surface. The effective tangential stress, τ, due to this effect on the free surface was calculated as follows:

$$\tau = f_l \frac{d\gamma}{dT}\nabla T \qquad (7)$$

where $d\gamma/dT$ is temperature coefficient of surface tension and f_l is the liquid fraction. The f_l is calculated from a relationship similar to the one given in equation (5). The multiplication of the shear stress with f_l takes into account the decrease in the

shear stress in the mushy region. The electromagnetic force, F_e, was calculated by the formulation given by Kou et al. [10].

The source term for enthalpy equation, S_h, considered the heat exchange between the surface of the sample and the heat source including the radiative and convective heat loss to the surrounding [20]. Along the plane of symmetry, the gradient of enthalpy was zero. At the other surfaces of the sample, the temperature was prescribed as the interpass temperature.

The governing equations were represented in a finite difference form and solved iteratively on a line-by-line basis using Tri-Diagonal Matrix Algorithm (TDMA). The Semi-Implicit Method for Pressure-Linked Equations (SIMPLE) algorithm was employed for the discreatization of the equations. The details of the procedure are described elsewhere [21]. The model used 65 X 39 X 17 spatially non-uniform grids for the calculation of enthalpy and velocity.

Calculation of Temperature-Time Data. From the steady state temperature field, obtained by the solution of conservation equations, temperature as a function of time at different locations (x,y,z) can be calculated by the following relation:

$$T(x,y,z,t2) = \frac{T(\xi 2,y,z) - T(\xi 1,y,z)}{\xi 2 - \xi 1} U_s (t2 - t1) + T(x,y,z,t1) \quad (8)$$

where T(ξ2,y,z) and T(ξ1,y,z) are the steady state temperatures at coordinates (ξ2,y,z) and (ξ1,y,z), respectively, (ξ2 - ξ1) is the distance traveled by the arc in time (t2 - t1), T(x,y,z,t1) and T(x,y,z,t2) are the temperatures at location (x,y,z) at times t1 and t2, respectively.

Phase Transformation Model. The low alloy steel weld metal microstructure consists of various ferrite morphologies such as allotriomorphic ferrite, Widmanstätten ferrite and acicular ferrite. A typical sequence of microstructure development in low alloy steel weld metal is given in Fig. 1. The model developed by Bhadeshia et al. [13,14,22] can predict volume percentage of above ferrite morphologies for a given weld metal composition and welding process variables. In this model, weld metal cooling rates are calculated for a given welding process conditions, using a semi-empirical approach developed by Svensson et al. [22]. To describe the cooling rates in 1100 to 700 K temperature range, Svensson et al. [22] measured the cooling rates experimentally by harpooning Pt, Pt-Rh thermocouples into the weld pool region of a standard ISO 2560 weld, for various welding conditions and processes. Then, they fitted the experimentally measured cooling rates to the following equation:

$$\frac{dT}{dt} = \frac{C_1 (T - T_i)^{C_2}}{q\eta} \quad (9)$$

where C_1 and C_2 are adjustable constants, T is the temperature of interest, T_i is the interpass temperature, q is the net welding heat input per unit length and η is the process efficiency. They assumed that the constants C_1 and C_2 to be independent of welding conditions and locations within the weld pool for a given welding process. Equation (9) was then used in the prediction of weld metal microstructure.

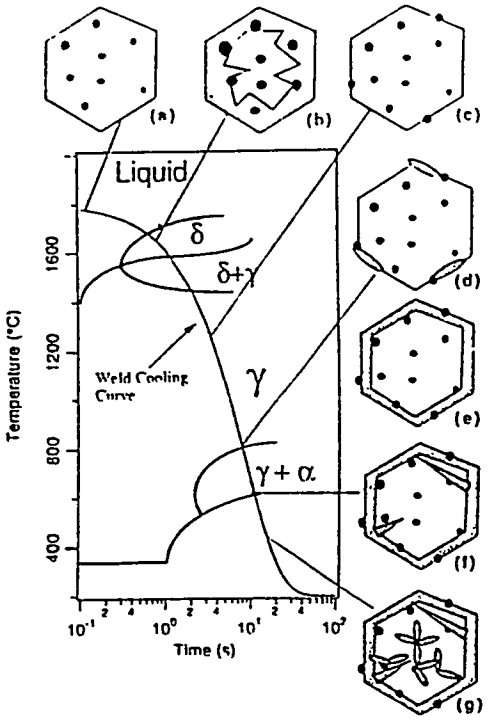

Fig. 1: Schematic diagram showing the development of weld metal microstrcture (a) inclusion formation, (b) solidification of liquid to ferrite, (c) fully austenitic structure, (d) nucleation of allotriomorhic ferrite, (e) growth of allotriomorhic ferrite along austenite grain boundaries, (f) Widmanstätten ferrite formation and (g) acicular ferrite formation.

The cooling rates obtained from equation (9) cannot be used for predicting microstructures in different locations within the weld. Furthermore, the constants C_1 and C_2 have to be determined for each set of experimental conditions. Therefore, in this work the cooling rates calculated from the solution of equations of conservation of mass, momentum and energy are coupled with the phase transformation model developed by Bhadeshia et al. [13] to predict the fusion zone microstructure.

Experimental Validation. The coupled fluid flow, heat transfer and microstructure model described above was used to predict microstructures for the experimental conditions published by Evans [23]. Evans has measured the volume fractions of ferrite morphologies in the top bead of multi-pass welds with different levels of V and Mn contents in Fe-C-Si low alloy steel welds. These weld beads were deposited by manual metal arc welding process with following conditions: welding voltage 21 V, welding current 170 A, welding speed 0.0027 m/s, and interpass temperature of 473 K. The weld joint geometry was in accordance with ISO 2560 joint [23]. For the above conditions, thermal histories at different locations in the weldment were predicted using the fluid flow and heat transfer model. The calculated cooling rates and the experimental austenite grain size data [23] were then used to calculate the microstructure within the fusion zone for all the weld metal compositions given in Table I.

Table I: Weld metal composition and austenite grain size, L, used in the calculations [23].

	C (wt %)	Si (wt%)	Mn (wt%)	V(wt%)	L, μm
1	0.073	0.35	0.64	0.0003	118
2	0.071	0.36	0.63	0.0210	94
3	0.071	0.40	0.64	0.0435	105
4	0.074	0.36	0.63	0.06	88
5	0.072	0.36	0.64	0.0815	95
6	0.077	0.31	1.33	0.0004	84
7	0.072	0.33	1.22	0.0190	92
8	0.077	0.26	1.36	0.0425	88
9	0.078	0.30	1.35	0.0595	82
10	0.076	0.26	1.36	0.1005	85

RESULTS AND DISCUSSION

Fluid Flow and Heat Transfer. The three dimensional steady state temperature field obtained by the solution of the ormed equations of conservation of mass, momentum and energy, for the manual metal arc welding of low alloy steels [23] is shown in Fig. 2. The peak temperature attained by the weldpool surface just below the arc was found to be 2490 K. The general features of the temperature field are consistent with the results reported in the literature [10] for a moving heat source. In front of the heat source, the temperature gradient is greater than that behind the heat source. This results inslightly greater liquid velocities in front of the heat source then behind the heat source. This can be observed from the velocity fields on the weld pool surface and along the plane of symmetry (y=0), presented in Fig. 2(b) and (c), respectively. The surface flow also shows that the liquid moves from the center (point of maximum temperature) to the periphery of the weld pool. This is expected for a metal with a very low concentration of surface active elements which will result in a negative temperature coefficient of surface tension, dγ/dT, over the weld pool surface. The temperature field show a typical elongated weld pool. Morever, the weld pool size was found to be similar to the experimental results of Evans [23].

The calculations show that, the length of the mushy zone at the trailing edge of the weld pool was longer than at all the other regions. The area of mushy zone controls the a extent of solute segregation and also the solidification features. The phase transformation model by Bhadeshia et al. [13], considers the solute segregation and takes this into account while calculating the TTT diagram. The solidification features may affect the prior austenite grain size within the weld pool. However, in the present work, experimentally measured austenite grain size were used and the variations in austenite grain size within the weld pool was assumed to be negligible.

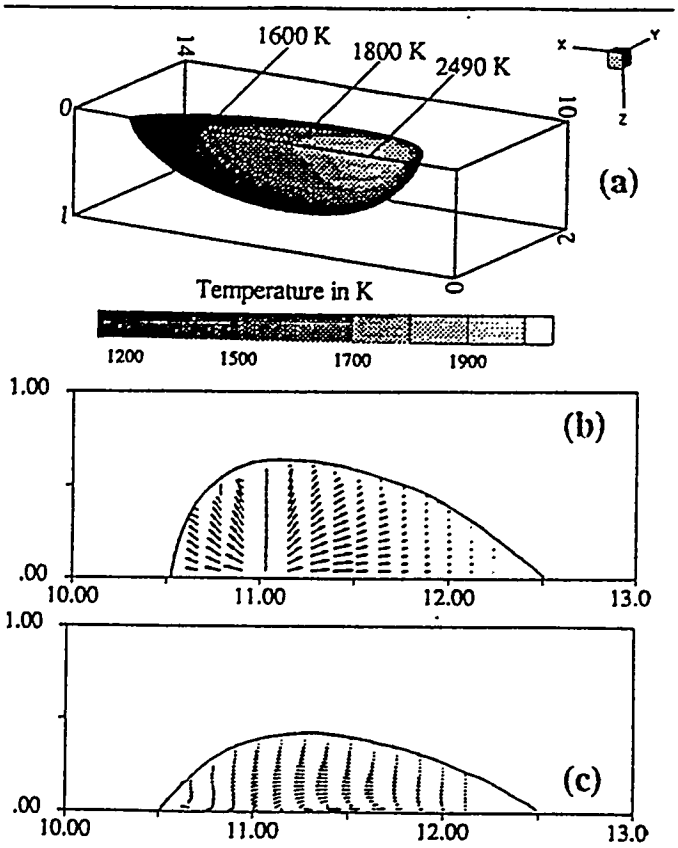

Fig. 2: Calculated results (a) temperature distribution and velocity vectors on (b) top surface, and (c) along plane of symmetry. Sample dimensions are in cm.

Thermal Cycles and Cooling Rates. From the computed temperature field, the thermal cycles were computed by equation (8). Fig. 3(a) shows the temperature contour profiles calculated by the model. The contour corresponding to solidus

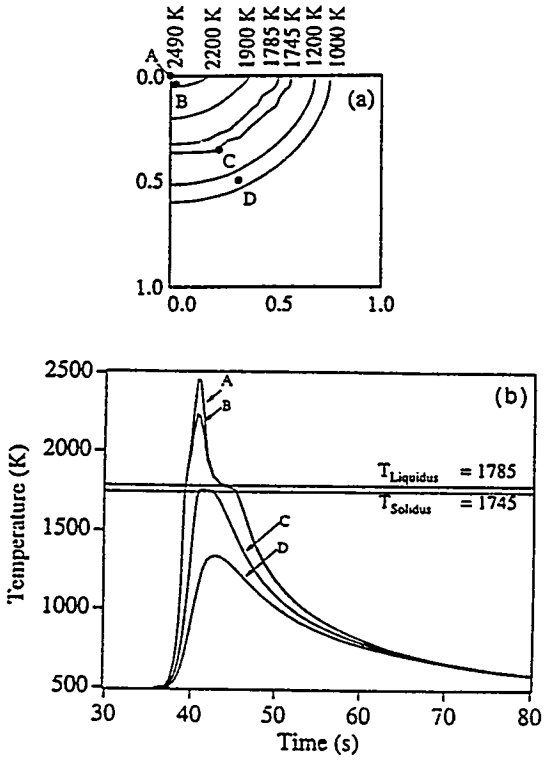

Fig. 3: Temperature contours and the four monitoirng locations (b) temperature-time data at the four locations.

tween the fusion line and the contour corresponding to liquidus temperature 1785 K, represents the mushy region. The temperature-time data at different locations (A, B, C & D) are shown in Fig. 3(b). The positions of these four points, on a cross section of the weldment normal to the welding direction, are marked in Fig. 3(a). The temperature-time data at any other cross-section, normal to the welding direction, will be same except for the time lag between the responses at the two cross-sections. The results in Fig. 3(b) show that thermal cycles vary at different locations. It is interesting from Fig. 3(b) that the peak temperatures are not reached at the same time at all locations. The time it takes for any point to attain its peak temperature depends on its distance from the heat source.

In this work, the cooling rates are computed at all locations of the weldment. Fig. 4 shows the cooling rates predicted by the present work as a function of temperature at various locations. The results shows that the difference in cooling rates at different locations are not significant in the temperature range of 1100 K to 700 K. Since there are no significant differences in the cooling rates as a function of position within the fusion zone, the spatial difference in microstructure is also expected to be negligible, which will be discussed later. Fig. 4 also shows the comparison of cooling rates predicted by the present work and by the semi-empirical approach [22], i.e., equation (9). The cooling rates predicted by this work Is higher than that predicted by equation (9). This difference in cooling rate will influence the microstructural prediction.

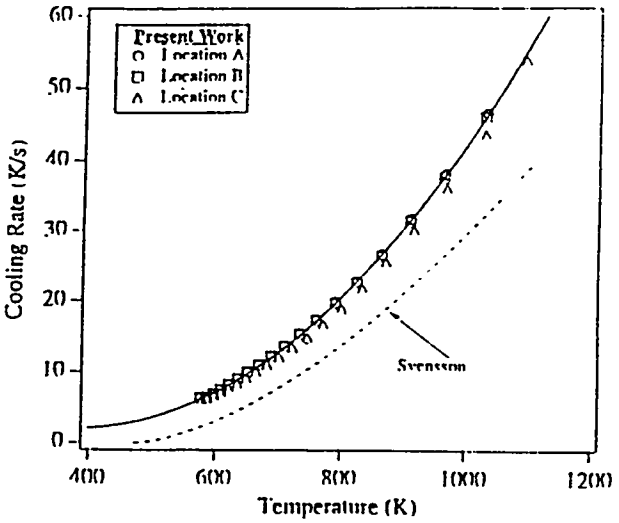

Fig. 4: Cooling rates at different locations within the fusion zone. The cooling rates predicted by Svensson et al. [22] is also shown for comparison.

Microstructural Calculation. The cooling rates predicted by the present work are used in calculating the volume percentages of ferrite morphologies in the fusion zone for various Fe-C-Mn-V steel weld compositions given by Evans [23]. The calculated microstructural constituents in the location B (Fig. 3 (a)) are compared with the experimental observations in Table 2. The table also contains the predictions by the original model of Bhadeshia et al. [13] where the cooling rates are predicted by equation (9). Since the cooling rates predicted by the present work are higher than that predicted by equation (9), the allotriomorphic ferrite percentage predicted by present work is slightly lower than that predicted by the Bhadeshia et al. model. On the whole, the calculations showed negligible spatial variations in the percentages of ferrite morphologies in different spatial variations in the percentages of ferrite morphologies in different locations due to the roughly identical cooling rates calculated at these locations. The present results evidently supports the assumption of Svensson et al. [22] that the variation in cooling rates within the fusion zone may not be significant enough to induce a drastic microstructural difference.

The comparison of overall predicted microstructural constituents with the experimental data showed slightly better correlation [18] than the calculations using original Bhadeshia et al. [13] model. It is important to note that the present work is the first attempt at coupling transport phenomena and a fundamental phase transformation models. The correlations between the predicted and the experimental data are expected to improve with refinement in the model. Since the semi-empirical approach used by Bhadeshia et al. [13] yields approximately similar results as that of present work, one may choose against comprehensive and computationally intensive transport phenomena models to describe the thermal cycles in the weldment. However, the semi-empirical approach [13] cannot be used directly for different geometry's, i.e. for every new welding conditions, the C_1 and C_2 have to be determined

Table II: Comparison of the experimental and predicted volume fractions of different ferrite morphologies.

	Allotriomorphic Ferrite			Widmanstätten Ferrite			Accicular Ferrite		
	Exn.*	Predicted		Exn.*	Predicted		Exn.*	Predicted	
No.		Present	Ref. 13†		Present	Ref. 13†		Present	Ref. 13†
1	48	31	34	27	20	19	25	49	47
2	45	37	43	15	27	25	40	36	32
3	42	34	39	7	24	23	51	42	38
4	36	41	44	6	25	24	58	34	32
5	35	36	39	7	24	24	58	40	37
6	23	30	34	7	15	14	70	55	51
7	26	33	35	2.5	16	16	71	51	49
8	23	28	32	5	13	13	72	59	55
9	20	30	34	4	13	13	76	57	52
10	12	29	33	3	13	12	85	58	54

* The experimental data are from reference 23, † These predictions are based on the model of Bhadeshia et al. [13]

experimentally. Also, this approach is incapable of calculating the spatial variation of weld metal cooling rates.

Spatial Variation of Microstructure. The above analysis showed no difference in the microstructural constituents at different locations. However, in some high alloyed steels welds, a small change in the cooling rates may lead to a different microstructure. This is illustrated with an example. The cooling rate calculations (Fig. 4) were applied to Fe-C-Cr-Mo (wt.%) weld. The results are presented in Table 3. The formation of allotriomorphic and Widmanstätten ferrite is predicted in location C, whereas in locations A & B 100% acicular ferrite is predicted. This is because the cooling rates at location A & B are slightly higher than the critical cooling rate for nucleation and growth of allotriomorphic ferrite at the austenite grain boundary. As a result, at these locations allotriomorphic ferrite formation is completely suppressed. At location C, the cooling rates are lower than the critical cooling rates leading to the formation of the allotriomorphic ferrite. Since there are no available experimental data on the spatial variation of the microstructural constituents within the fusion zone, the above predictions can not be validated. However, such calculations can be used in the theoretical design of weldment and welding procedures. For example, it has been reported that in cases where allotriomorphic ferrite formation is completely suppressed (e.g., at locations A & B), the acicular ferrite microstructure may be replaced by bainitic microstructure [24]. The bainitic microstructure is deleterious to the weld metal properties. However, by changing the weld composition or weld metal cooling conditions, bainitic microstructure development can be suppressed and acicular ferrite microstructure may be promoted [24].

Table 3: Calculated microstructural constituents at different locations for Fe-.07C-0.45Si-1.0Mn-0.5Ni-2.25Cr (wt%) weld.

	Ferrite Volume %		
Locations	Allotrimorphic	Widmanstätten	Acicular
A	0	0	100†
B	0	0	100†
C	11	5	84

† In these cases, the microstructure consists of mixture of acicular ferrite, bainite and martensite.

SUMMARY AND CONCLUSION

A numerical computational model to describe the heat transfer and fluid flow in welds has been developed. The fluid flow and heat transfer model predicted a small variation in the cooling rates at different locations within the fusion zone. The calculated cooling rates were coupled with an existing phase transformation model to predict the volume percentages of different ferrite morphologies in ten different Fe-C-Mn-V low alloy steel welds. The computed microstructural results are in agreement with independent experimentally data. The small variations in the cooling rates at different locations in the fusion zone did not result in significant spatial variations of the microstructure in the fusion zone. Calculations indicate that a small difference in cooling rates, for certain weld compositions, may result in significant microstructural variation in the weldment. The above calculation features and the agreement between experimental and predicted measurements indicates significant promise for predicting weld metal microstructure distribution by coupling the fundamentals of transport phenomena with the phase transformation models.

ACKNOWLEDGMENTS

The authors are grateful to Dr. H. K. D. H. Bhadeshia, University of Cambridge, UK for allowing the authors to use his computer program to predict the steel welds microstructures. This work was supported by the U.S. Department of Energy, Office of Basic Energy Sciences, Division of Materials Science, under grant numbers DE-FG02-84ER45158 with Pennsylvania State University and DE-AC05-84OR21400 with Lockheed Martin Energy Systems, Inc.

REFERENCES

1. S. A. David and T. DebRoy, Science, 257 (1992), 497.
2. T. DebRoy and S. A. David, Rev. of Mod. Phys.,(in press).
3. H. G. Kraus, Weld. J, 68 (1989), 269s.
4. D. Rosenthal, Trans. ASME, 68 (1946), 829.
5. C. M. Adams. Jr., Weld. J, 37 (1958), 211s.
6. E. Friedman, Trans. ASME J. Press. Vessel Techn., 97 Series J (3) (1975), 206.
7. G. Oreper and J. Szekely, J. of Flu.. Mech., 147 (1984), 53.
8. C. Chan, J. Mazumder and M. M. Chen, Met. Trans, 15A (1985), 217.
9. A. Paul, and T. DebRoy, Met. Trans., 19B (1988), 851.
10. S. Kou, and Y. Wang, Met. Trans, 17A (1986), 2265.
11. T. Zacharia, S. A. David, J. M. Vitek and T. DebRoy, Weld. J., 68 (1989), 499.
12. W. Pitscheneder, T. DebRoy, K. Mundra, and R. Ebner, Submitted to Weld. J, 1994.
13. H. K. D. H. Bhadeshia, L. E. Svensson and B. Gretoft, Acta. Metall., 33 (1985), 1271.
14. H. K. D. H. Bhadeshia, International Trends in Welding Science and Technology, Eds. S. A. David and J. M. Vitek, ASM International Park, Ohio, 1993, pp.213-222.
15. S. Babu, S. A. David, J. M. Vitek, K. Mundra and T. DebRoy, Materials Science and Technology, in press.
16. S. A. David and J. M. Vitek, see reference 15, 147-156.
17. K. Mundra and T. DebRoy, Unpublished work, The Pennsylvania State University, 1994.
18. K. Mundra, T. DebRoy, S. Babu and S. A. David, Submitted to Welding Journal.
19. V. R. Voller, and C. Prakash, Intl. J. Heat Mass Transfer, 30 (1987), 1709-1719.
20. K. Mundra and T. DebRoy, Met. Trans, 24B (1993), 145.
21. S. V. Patankar, Numerical Heat Transfer and Fluid Flow (N. Y.: Hemisphere Publication Corp, 1980).
22. L. E. Svensson, B. Gretoft and H. K. D. H. Bhadeshia, Scand. J. of Metall. 15 (1986), 96.
23. G. M. Evans, OERLIKON-Schweißmitt, 49 (1991), 18-33.
24. S. S. Babu and H. K. D. H. Bhadeshia, Mater. Sci. and Technol., 6 (1990), 1005-1020.

DISCLAIMER